JASA ARTICLE

Physics of phonation offset: Towards understanding relative fundamental frequency observations

Mohamed A. Serry,[1] Cara E. Stepp,[2,a)] and Sean D. Peterson[1,b)]
[1]Department of Mechanical and Mechatronics Engineering, University of Waterloo, Waterloo, Ontario N2L 3G1, Canada
[2]Department of Speech, Language & Hearing Sciences, Boston University, Boston, Massachusetts 02215, USA

ABSTRACT:
Relative fundamental frequency (RFF) is a promising assessment technique for vocal pathologies. Herein, we explore the underlying laryngeal factors dictating RFF behaviours during phonation offset. To gain physical insights, we analyze a simple impact oscillator model and follow that with a numerical study using the well-established body-cover model of the vocal folds (VFs). Study of the impact oscillator suggests that the observed decrease in fundamental frequency during offset is due, at least in part, to the increase in the neutral gap between the VFs during abduction and the concomitant decrease in collision forces. Moreover, the impact oscillator elucidates a correlation between sharper drops in RFF and increased stiffness of the VFs, supporting experimental RFF studies. The body-cover model study further emphasizes the correlation between the drops in RFF and collision forces. The numerical analysis also illustrates the sensitivity of RFF to abduction initiation time relative to the phase of the phonation cycle, and the abduction period length. In addition, the numerical simulations display the potential role of the cricothyroid muscle to mitigate the RFF reduction. Last, simplified models of phonotraumatic vocal hyperfunction are explored, demonstrating that the observed sharper drops in RFF are associated with increased pre-offset collision forces.
 https://doi.org/10.1121/10.0005006
(Received 15 October 2020; revised 15 April 2021; accepted 21 April 2021; published online 27 May 2021)
[Editor: Zhaoyan Zhang] Pages: 3654–3664

I. INTRODUCTION

In recent years, voice researchers have strived to develop acoustic measures to assess and classify voice disorders without the need to conduct extensive clinical examinations of the larynx (Henríquez *et al.*, 2009; Jiang *et al.*, 2009; Jiang *et al.*, 2006). One promising tool that has gained research interest recently due to its potential assessment capabilities is the relative fundamental frequency (RFF) of phonation surrounding voiceless consonants (Goberman and Blomgren, 2008; Heller Murray *et al.*, 2020; Stepp *et al.*, 2010). Frequency characteristics during the transition from the first vowel to the obstructing consonant and then to the second vowel vary significantly (Hanson, 2009; Ohde, 1984; Watson, 1998), and the differences in the vocal mechanisms altering these characteristics among healthy and pathological speakers may contribute to the assessment ability of RFF (Heller Murray *et al.*, 2017).

In clinical evaluations, RFF analysis is conducted on acoustic signals from microphone recordings (Stepp *et al.*, 2010; Watson, 1998), or on acceleration signals from neck measurements (Lien *et al.*, 2015), where phonation cycles surrounding voiceless consonants are detected either manually, which is the standard, or semi-automatically (Lien *et al.*, 2017; Vojtech *et al.*, 2019). Twenty cycles are then considered in the analysis, with ten cycles for the offset part of phonation (phonation prior to the voiceless consonant) and ten cycles for the onset part (phonation following the voiceless consonant). The fundamental frequency of these cycles is determined from the signal peaks and the RFF, a normalized measure of frequency in the form of semitones, is computed as

$$\mathbf{RFF}(f) = 12\log_2\left(\frac{f}{f_{\mathbf{ref}}}\right), \tag{1}$$

where f denotes the fundamental frequency and $f_{\mathbf{ref}}$ denotes the fundamental frequency of the reference cycle. For phonation offset, $f_{\mathbf{ref}}$ is the first cycle, whereas the tenth cycle is used for phonation onset.

In general, healthy and pathological speakers exhibit a drop in RFF during phonation offset and a spike in RFF followed by a decay during phonation onset (Stepp *et al.*, 2010). Adult speakers with voice disorders and aged speakers exhibit sharper drops in RFF during offset in comparison to adult speakers with healthy voices and young speakers, respectively (Stepp *et al.*, 2010; Watson, 1998). Similarly, these groups also exhibit relatively smaller initial values of RFF during phonation onset. Interestingly, such differences between healthy and pathological voices are less apparent in the case of pediatric speakers (Heller Murray *et al.*, 2020).

The physics of phonation offset is extremely complex due to its transient nature and the involvement of various

a)ORCID: 0000-0002-8045-252X.
b)Electronic mail: peterson@uwaterloo.ca, ORCID: 0000-0001-8746-2491.

https://doi.org/10.1121/10.0005006

laryngeal, aerodynamic, and acoustic factors. During offset, laryngeal muscles abduct the vocal folds (VFs) and alter their mechanical properties (vibrating mass, stiffness, etc.), which induces a gradual transition from a collision to non-collision regime (Diaz-Cadiz *et al.*, 2019). A number of studies have attempted to elucidate the physics of phonation offset. Smith and Robb (2013) conducted an experimental analysis on utterances of different aerodynamic characteristics and suggested that laryngeal and aerodynamic factors are equally important in varying frequency during phonation offset. They further suggested that the drop in RFF during offset may be attributed to a decrease in the VF stiffness. Jaiswal (2011) investigated clinically the role of the cricothyroid (CT) muscle during offset and found that the CT activation increase during offset is not consistent among all speakers. Watson (1998) analyzed the differences in RFF trends between young and older adult speakers and hypothesized that the drop in RFF during offset is attributed to biomechanical factors and, in particular, the decrease in collision forces associated with abduction. Lucero and Koenig (2005) employed inverse analysis, with oral aerodynamic measurements during the /ihi/ utterance as the observation data and a two mass model for the fitting, and found a decrease in the sub-glottal pressure and an increase in the VF stiffness during offset. They did not, however, elucidate the mechanisms altering frequency during such phonation periods.

These prior studies, while offering insights into phonation offset and RFF, do not rigorously explore the physics of frequency changes and RFF during phonation offset. This is due to the fact that these prior studies were either qualitative in nature, reliant on a small number of data points, and/or based on experimental procedures that result in highly variable measurements due to uncontrolled laryngeal, aerodynamic, and acoustic factors. Controlling and quantifying such factors during experimental analysis of phonation offset is extremely challenging and thus, in this work, we adopt analytical and numerical approaches in an effort to explain some of the underlying factors altering frequency and RFF during phonation offset. We note that the literature is rich in analytical studies of the frequency characteristics of the VFs (Berry and Titze, 1996; Titze, 1989; Titze and Hunter, 2004; Zhang *et al.*, 2006). However, to the best knowledge of the authors, the theoretical treatment in this work is the first that considers the role of collision on fundamental frequency, especially during phonation offset.

The organization of this work is as follows: Sec. II is an analytical examination of the driving factors affecting fundamental frequency during phonation offset using a single degree-of-freedom impact oscillator; Sec. III extends the analysis to a body-cover model of the VFs, enabling exploration of laryngeal factors, such as muscle activation and abduction duration, and scenarios associated with phonotraumatic vocal hyperfunction; and the paper concludes with a summary and discussion of future work in Sec. IV.

II. INSIGHTS FROM A SIMPLE IMPACT OSCILLATOR

We begin the examination of frequency variations during phonation offset via analysis of a simplified one degree-of-freedom impact oscillator. This model embeds the pertinent physical parameters (e.g., mass, stiffness, neutral gap, and collision elasticity) yet is analytically tractable. Impact oscillators arise in a variety of physical systems, including bouncing balls (Nagurka and Huang, 2004), vibratory plows (Senator, 1970), and rolling ships interacting with icebergs (Grace and Ibrahim, 2008), and have been extensively studied numerically, experimentally, and analytically (Ing *et al.*, 2008; Nordmark, 1991; Shaw and Holmes, 1983).

A. Impact oscillator model

Consider the impact oscillator model shown in Fig. 1, where M is the mass, K is the body stiffness, $\delta \geq 0$ is the neutral gap (distance from the collision plane to the rest position of the mass), and $k_{\mathbf{col}}$ is the collision stiffness. We assume that the mass is initially at the rest position $\xi(0) = 0$ moving in the positive direction with kinetic energy E_0. Consequently, the initial velocity is given by $v_0 = \sqrt{2E_0/M}$. The kinetic energy E_0 corresponds to the aerodynamic energy transferred from the intra-glottal flow to the VFs. Herein, we implicitly implement a quasi-static assumption as it was observed clinically that VF abduction is slow relative to phonation frequency [the abduction period is about 80 ms, whereas the phonation period is less than 10 ms (Diaz-Cadiz *et al.*, 2019)]. The governing equations of the impact oscillator are

$$M\ddot{\xi} + K\xi = 0, \quad \xi(t) \geq -\delta, \tag{2}$$

$$M\ddot{\xi} + K\xi + k_{\mathbf{col}}(\xi + \delta) = 0, \quad \xi(t) < -\delta. \tag{3}$$

To ensure the occurrence of collision after the oscillator crosses the rest position, we impose the condition $0 \leq \tilde{\delta} \leq 1$, where $\tilde{\delta} = \sqrt{K/(2E_0)}\delta$ is the normalized neutral gap.

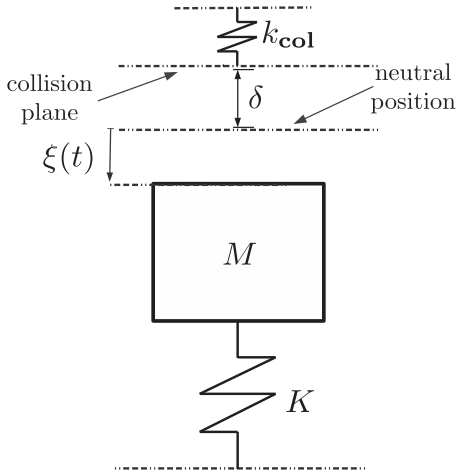

FIG. 1. Schematic of the impact oscillator system.

B. Frequency analysis

The motion of the impact oscillator is periodic, as shown schematically in Fig. 2. During each period, the impact oscillator spends t_c in the collision regime, t_f when $\xi(t) \geq 0$, and $2t_\delta$ between the neutral position and the collision plane, where t_δ is the time required to move from the neutral position to the collision plane (see Fig. 2). The fundamental frequency of the oscillator is then given by $f = (t_c + t_f + 2t_\delta)^{-1}$. Substituting the closed-form relations of t_c, t_f, and t_δ (see Appendix A) yields

$$f = \frac{2f_0}{\frac{2}{\pi}\sqrt{\tilde{k}}\arctan\sqrt{\frac{\left(1/\tilde{\delta}^2\right)-1}{\tilde{k}}} + \frac{2}{\pi}\arcsin\tilde{\delta} + 1}, \quad (4)$$

where $f_0 = \sqrt{K/M}/(2\pi)$ is the natural frequency of the oscillator and $\tilde{k} = K/(K + k_{\mathbf{col}})$ is the normalized stiffness.

Note that the stiffness in the collision regime governed by Eq. (3), $K + k_{\mathbf{col}}$, is larger than the stiffness in the non-collision regime [Eq. (2)], K, while the mass remains unchanged. Hence, spending more time in the collision phase increases the system frequency. The fundamental frequency satisfies the bounds $f_0 \leq f \leq 2f_0$ (see Appendix B), which indicates that fundamental frequency of the impact oscillator is larger than or equal to its natural frequency, with a theoretical upper bound being double the natural frequency. The limiting values of f can be inferred by considering the cases of (a) a rigid impact ($k_{\text{col}} \to \infty$) and no gap ($\delta = 0$), which results in a rectified version of the basic oscillator, and hence a fundamental frequency of $2f_0$; and (b) a large gap ($\tilde{\delta} > 1$) and/or infinitely compliant collision ($k_{\text{col}} = 0$), which would result in the basic oscillator without alteration, and hence a fundamental frequency of f_0.

C. Parameters influencing frequency

In this subsection, we illustrate the role of the body and collision stiffnesses and the neutral gap in altering fundamental frequency. Figure 3 shows that the normalized

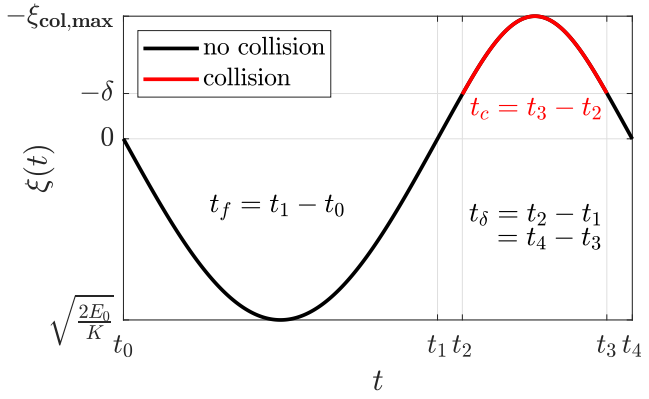

FIG. 2. (Color online) Periodic behaviour of the impact oscillator; $\xi_{\mathbf{col,max}} = \delta + \eta_{\mathbf{max}}$, where $\eta_{\mathbf{max}}$ is defined in Appendix C.

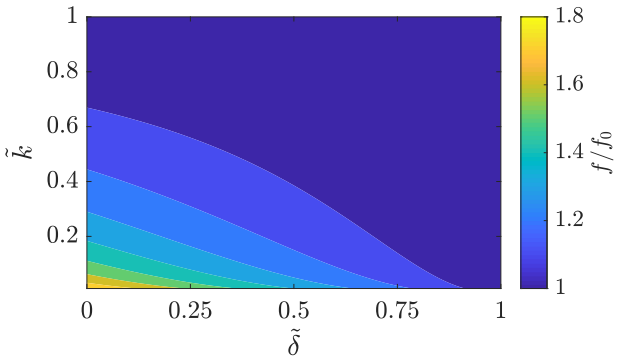

FIG. 3. (Color online) Contour plot of f/f_0 as a function of the normalized neutral gap $\tilde{\delta}$ and normalized stiffness $\tilde{k}$.

fundamental frequency f/f_0 decreases with increasing $\tilde{k}$ and $\tilde{\delta}$. Physically, this indicates that fundamental frequency is proportional to collision stiffness $k_{\mathbf{col}}$ and inversely proportional to the neutral gap δ. The relation between f/f_0 and $\tilde{\delta}$ also highlights the role of E_0, corresponding to aerodynamic energy transfer to the VFs, wherein an increase in the energy input leads to higher fundamental frequency. This agrees with the findings of previous studies, which showed a positive correlation between fundamental frequency and transglottal pressure (Titze, 1989). Equations (2) and (3) further state that increasing the body stiffness K increases f, whereas Eq. (4) and the formula of f_0 indicate that increasing the mass decreases the fundamental frequency as $f \propto M^{-0.5}$. Projecting these relations onto clinical data, we conclude the following: During offset, the VFs transition gradually from a collision to non-collision regime, where the frequency in the collision regime is generally higher than the frequency in the non-collision regime (natural frequency). This shift explains the drop in fundamental frequency or RFF observed clinically. Moreover, activating different laryngeal muscles during offset changes the mechanical properties of the VFs (stiffness, mass, neutral gap, etc.), which consequently alters profiles of fundamental frequency and RFF.

D. Collision forces and frequency

In this subsection, we illustrate the correlation between fundamental frequency and collision forces. The correlation between collision forces and fundamental frequency was suggested previously by Watson (1998) to explain the clinical RFF observations of aged speakers. By direct computations (see Appendix C), we obtain the following for the maximum collision force, defined as

$$F_{\mathbf{col,max}} = F_{\mathbf{e,max}}(1 - \tilde{k})\left(-\tilde{\delta} + \sqrt{\tilde{\delta}^2 + \frac{1 - \tilde{\delta}^2}{\tilde{k}}}\right), \quad (5)$$

where $F_{\mathbf{e,max}} = \sqrt{2E_0K}$ is the maximum elastic force in the non-collision regime. A contour plot of $F_{\text{col,max}}/F_{\text{e,max}}$ versus $\tilde{\delta}$ and $\tilde{k}$ is presented in Fig. 4. By comparing Figs. 3 and 4, it can be seen that fundamental frequency and

https://doi.org/10.1121/10.0005006

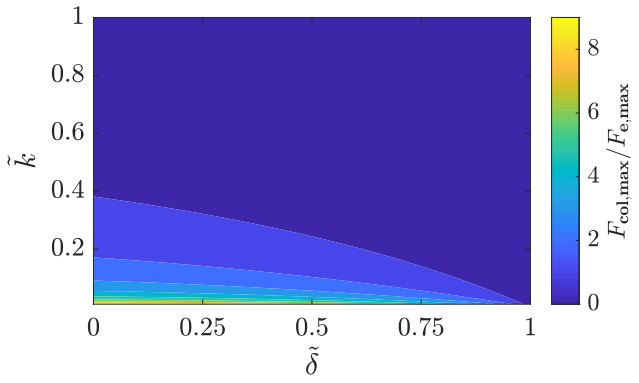

FIG. 4. (Color online) Contour plot of $F_{\mathbf{col,max}}/F_{\mathbf{e,max}}$ as a function of the normalized neutral gap $\tilde{\delta}$ and normalized stiffness $\tilde{k}$.

maximum collision force are correlated, as the effects of $\tilde{k}$ and $\tilde{\delta}$ on f/f_0 are similar to their effects on $F_{\mathbf{col,max}}/F_{\mathbf{e,max}}$. This suggests that experimental observations of RFF are correlated with the variation in collision forces. However, we note that the fundamental frequency does not depend solely on collision forces. This can be observed, for example, from the fact that the mass affects the fundamental frequency, but it does not alter the maximum collision force, as seen in Eqs. (4) and (5). The correlation between fundamental frequency and collision forces will be further explored numerically in Secs. III C and III E.

E. Parameters influencing relative frequency

In Secs. II A–II D, we analyzed the different factors altering fundamental frequency. In this subsection, we focus on fundamental frequency relative to the frequency at the fully adducted state, $f|_{\delta=0}$. Physically, this relates to RFF during phonation offset, as it compares the frequency in one state with that at the fully adducted state (e.g., during a sustained vowel). It can be seen from Fig. 5 that the frequency ratio $f/f|_{\delta=0}$ is always less than or equal to 1, as the fundamental frequency is maximum at the fully adducted state $\delta = 0$. Moreover, the frequency ratio decreases with increasing $\tilde{\delta}$ due to reduced time in the collision phase as the neutral gap increases. This agrees with clinical data that

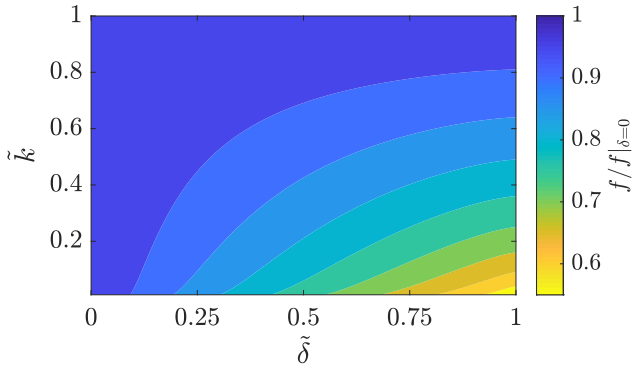

FIG. 5. (Color online) Contour plot of frequency ratio $f/f|_{\delta=0}$ as a function of the normalized neutral gap $\tilde{\delta}$ and normalized stiffness $\tilde{k}$.

shows RFF decreasing during offset as the VFs are abducted. Moreover, $f/f|_{\delta=0}$ increases as $\tilde{k}$ increases, which is attained by decreasing $k_{\mathbf{col}}$. For small collision stiffness, frequency is primarily determined by body stiffness K and thus, fundamental frequency is approximately equal to the natural frequency. In the case of real VFs, collision stiffness is significant (Steinecke and Herzel, 1995; Story and Titze, 1995). Hence, collision forces constitute a major factor altering the fundamental frequency. The role of body stiffness in altering relative frequency is complex as K affects $\tilde{\delta}$ and $\tilde{k}$ in opposing ways. However, by letting the collision stiffness $k_{\mathbf{col}}$ be dependent on the body stiffness, say $k_{\mathbf{col}} = \alpha K$ for some constant $\alpha > 0$ [see, e.g., Steinecke and Herzel (1995) and Story and Titze (1995)], then $\tilde{k} = 1/(1+\alpha)$. Hence, the body stiffness does not alter the stiffness ratio $\tilde{k}$ when $k_{\mathbf{col}}$ depends on K linearly. However, the body stiffness K increases $\tilde{\delta}$ and consequently lowers the relative frequency values. This implies the correlation between increased stiffness of the VFs and sharper drops in RFF, supporting the findings from previous experimental studies (McKenna *et al.*, 2016).

III. BODY-COVER VOCAL FOLD SIMULATIONS

Section II introduced a simplified theoretical analysis of phonation offset that ignored the physiological aspects of the VFs and their transient nature during such phonation periods. In this section, we adopt a more physiologically relevant model, namely the three-mass body-cover model (Story and Titze, 1995) and carry out a numerical study exploring a variety of physical parameters, including muscle activation, abduction timing, and vibrating mass. This model is selected for its blend of relative simplicity coupled with demonstrated success in modeling several phonation scenarios (Erath *et al.*, 2013; Story, 2002; Zañartu *et al.*, 2014).

A. Body-cover model

Figure 6 shows a schematic diagram of the body-cover model used in this study. This model, which embeds the essential physiological components of the VFs employed during modal voice, consists of two cover masses, m_1 and m_2, and a body mass, m_b, all connected via springs and dampers to model tissue viscoelasticity. The resting positions of the masses result in a nearly rectangular glottal configuration with a neutral glottal gap given by x_0. The model assumes the motion of the VFs to be symmetric about the medial plane. Collision of the opposing folds is modelled by activating additional nonlinear spring forces applied to the cover masses, where the spring force is proportional to the degree of overlap of the cover masses with the medial (collision) plane. We note here, unlike the implementation of Story and Titze (1995), that the damping coefficients are not increased during collision. The model employs muscle activation rules to control the primitive model variables (Titze and Story, 2002), wherein three muscle activation parameters, namely, $a_{\mathbf{CT}}$, $a_{\mathbf{TA}}$, and $a_{\mathbf{LCA}}$, account for the activation of the CT, thyroarytenoid (TA), and lateral/posterior

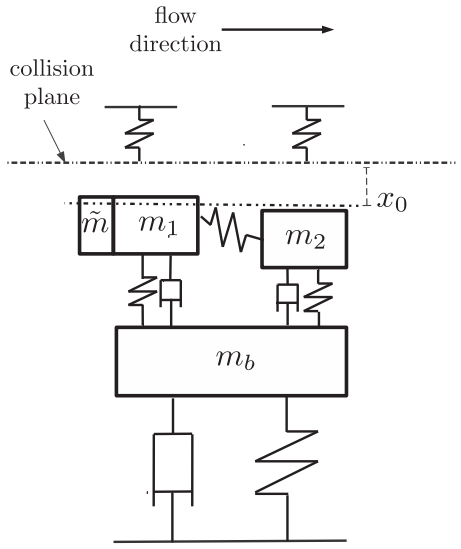

FIG. 6. Schematic diagram of the body-cover model.

cricoarytenoid (LCA/PCA) muscles, respectively. Moreover, a sub-glottal tract (Weibel *et al.*, 1963) and a supra-glottal tract, configured to simulate the /i/ vowel (Takemoto *et al.*, 2006), are included. The acoustics are modeled using wave reflection analog (Kelly and Lochbaum, 1962; Liljencrants, 1985; Story, 2005), where outward travelling pressure waves are multiplied by attenuation factors to account for losses, similar to implementations employed by Titze and Alipour (2006) and Zanartu (2006). The intra-glottal flow is simulated using the Bernoulli flow model. The body-cover model governing equations (Story and Titze, 1995) are solved numerically using an explicit version of Newmark's method (Newmark, 1959), which has previously been employed in studies involving discrete-time solutions of the body cover model (Galindo *et al.*, 2017; Galindo *et al.*, 2014; Hadwin *et al.*, 2016). The numerical scheme can be described briefly as follows: let $\mathbf{x}_i$, $\mathbf{v}_i = \dot{\mathbf{x}}_i$, and $\mathbf{a}_i = \dot{\mathbf{v}}_i$ denote the vectors of estimated displacements, velocities, and accelerations, respectively, of the body-cover model masses at some time step i, where $\mathbf{a}_i$ is computed from the momentum balance given $\mathbf{x}_i$ and $\mathbf{v}_i$. At the next time step, $i+1$, the displacements and velocities are computed from the kinematic relations $\mathbf{x}_{i+1} = \mathbf{x}_i + \mathbf{v}_i\tau + \mathbf{a}_i(\tau^2/2)$ and $\mathbf{v}_{i+1} = \mathbf{v}_i + \mathbf{a}_i\tau$, where τ is a fixed time step size associated with the sampling frequency, herein set to 70 kHz. A convergence study indicated that steady state oscillation frequency and offset frequency patterns differed by less than 1% in comparison with simulations at a sampling frequency of 350 kHz, and was thus deemed sufficiently resolved for the present study.

The passive model parameters employed, including VF length, correspond to a male speaker (Titze and Story, 2002). The simulations span 1.1 s, where all the model parameters are fixed during the first second to ensure that steady state sustained oscillations are achieved. After the initial one second, offset is initiated by varying muscle activation parameters in the remaining 0.1 s. Tables I and II list the variables and controlled parameters of interest in this study. Note that the maximum collision forces, $\max(F_{\mathbf{col},i})$, $i = 1, 2$, in Table I are estimated during the steady state oscillations.

TABLE I. Variables of interest in the current study.

Variable	Definition
A_g	glottal area
$F_{\mathbf{col},1}$	collision force of lower cover mass
$F_{\mathbf{col},2}$	collision force of upper cover mass
$F_{\mathbf{col,max}}$	$\max\{\max(F_{\mathbf{col},1}), \max(F_{\mathbf{col},2})\}$
f	fundamental frequency
x_0	neutral position
t	time

B. Signal analysis

In this work, we consider the time-series of the glottal area, A_g, instead of acoustic signals in our frequency analysis. We are concerned with fundamental frequency, which is directly obtained from the glottal area waveform without the confounds of higher frequency content present in the acoustic signal. To facilitate instantaneous frequency estimation, we modify the glottal area signals by subtracting the nominal (resting) area $2Lx_0$, where L is the length of the VF. We note here that the resting area is time-varying during offset simulations. Fundamental frequency is estimated from the peaks of the modified signal by identifying the times of two subsequent peaks, say t_{j-1} and t_j, and computing $f(t_j) = (t_j - t_{j-1})^{-1}$. We measure the differences between consecutive peaks and nadirs of the modified signal, which in general decay during phonation offset, and the last offset cycle is determined to be the cycle associated with a peak-to-nadir difference less than a threshold set to be 10% of the peak-to-nadir difference during sustained oscillations (see Fig. 7). If such a criterion is not met by the end of the simulation time, the last offset cycle is selected to be the last cycle detected in the simulation. Finally, once frequencies are estimated, RFF is calculated using Eq. (1), where the reference frequency $f_{\mathbf{ref}}$ is set to be the phonation fundamental frequency during the steady state oscillations.

C. Quasi-static analysis

We begin our numerical study with a quasi-static preliminary analysis to gain deeper insight into the effect of

TABLE II. Controlled parameters and their default values.

Parameter	Definition	Default value
$a_{\mathbf{CT}}$	CT activation	0.2
$a_{\mathbf{TA}}$	TA activation	0.2
$a_{\mathbf{LCA}}$	LCA/PCA activation	$\in [0.3, 0.5]$
P_s	static sub-glottal pressure	1000 Pa
t_i	abduction initiation time	1020 ms
$T_{\mathbf{abd}}$	abduction period	80 ms

https://doi.org/10.1121/10.0005006

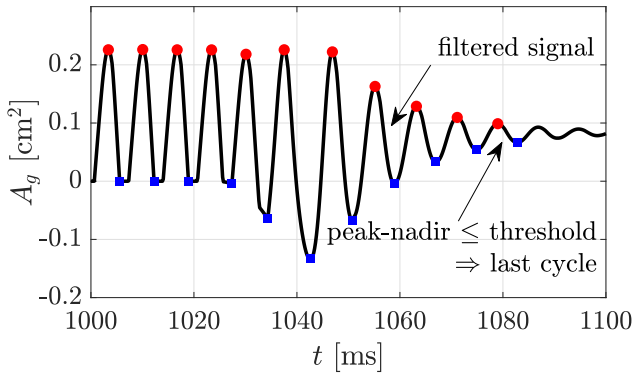

FIG. 7. (Color online) Modified glottal area profile with estimated location of the last offset cycle.

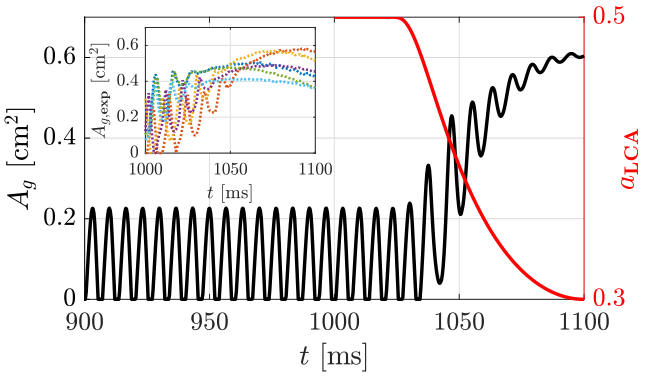

FIG. 9. (Color online) Estimated a_{LCA} profile and simulated glottal area based on empirical data of glottal area during the offset portion of the /ifi/ utterance. The inset shows empirical data extracted from a healthy male subject.

neutral gap, x_0, and collision forces on phonation fundamental frequency during sustained oscillations. Specifically, we record the neutral gap, fundamental frequency, and collision forces across several values of a_{LCA}. Figure 8 presents the effect of LCA muscle activation on the neutral gap, showing that as LCA activates it adducts the folds, which leads to a higher fundamental frequency in accordance with the findings in Sec. II. This follows the empirical relation introduced by Titze and Story (2002), $x_0 = 0.25L_0(1 - 2a_{\mathrm{LCA}})$, where L_0 is the un-stretched length of the VFs. Included as an inset in Fig. 8 are the maximum collision forces for m_1 and m_2 as a function of a_{LCA}. This highlights that the increase in fundamental frequency is correlated with the increase in maximum collision forces. This observation supports our hypothesis and the findings from Sec. II that the variation in fundamental frequency, especially during offset, is associated with the change in collision forces. This will be revisited in Sec. II E, where transient abduction gestures are considered.

D. Offset simulations

In order to model offset with the body-cover model, we employ experimental measurements to calibrate and set an appropriate a_{LCA} profile. Specifically, we extract the glottal angle, $\theta_{g,\mathrm{exp}}$, as a function of time for a healthy male speaker during the offset portions of repeated /ifi/ utterances[1] (Diaz-Cadiz *et al.*, 2019). We estimate the glottal area of the experiments, $A_{g,\mathrm{exp}}$, by assuming the glottis to be a circular sector, and thus $A_{g,\mathrm{exp}} = L_{\mathrm{male}}^2\theta_{g,\mathrm{exp}}/2$, where $L_{\mathrm{male}} = 1.6$ cm is the typical length of a male VF. The LCA muscle activation profile is then tuned to match the experimental glottal area estimates. Reasonable abduction levels are obtained with an a_{LCA} profile that decreases from 0.5 to 0.3 over an offset period estimated to be 80 ms. This LCA profile will be used in all offset simulations unless otherwise stated. Figure 9 shows how the simulated glottal area, based on the tuned LCA profile, varies in time. Included as an inset are the empirical data, which exhibit similar glottal areas and abduction duration.

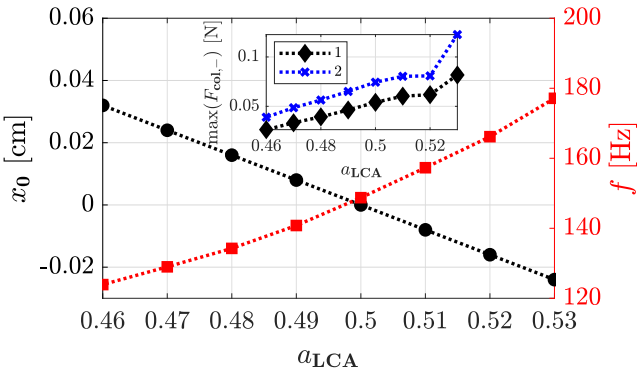

FIG. 8. (Color online) Neutral gap and phonation frequency vs LCA activation and the associated maximum collision forces.

E. Exploring the role of collision on RFF

In this subsection, we examine our hypothesis that RFF curve shape is largely driven by changes in the degree of collision. During offset, the time instance corresponding to the cessation of collision is identified as the first period for which the nadir of the original glottal area signal is nonzero. Figure 10 presents RFF and collision force for the exemplar case $(a_{\mathrm{CT}}, a_{\mathrm{TA}}) = (0.3, 0.3)$. The RFF curve initially decays while collision forces are non-zero, followed by a minimum value, denoted by $\mathbf{RFF}(f_{\mathrm{min}})$, and subsequent increase in RFF, with last detected value being denoted $\mathbf{RFF}(f_{\mathrm{last}})$,

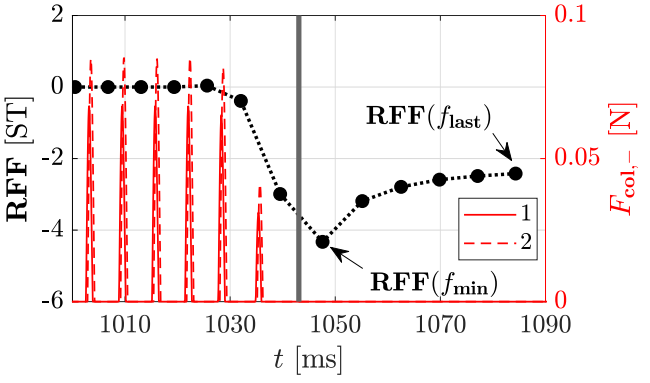

FIG. 10. (Color online) RFF and collision forces over time for $(a_{\mathrm{CT}}, a_{\mathrm{TA}}) = (0.3, 0.3)$. Vertical thick line indicates the detection of collision cessation.

when no collision forces are present. The figure shows correlation between the variation of the collision forces and the RFF profile, especially prior to collision cessation, which supports the main hypothesis of this work. After cessation of collision, the rise in RFF can be attributed to various transient effects including aerodynamics and abduction initiation time relative to phonation cycle. We note that this dip in the RFF profile has been observed experimentally within subjects, as seen in Fig. 11, but it is unknown whether this rise is associated with the cessation of collision. Furthermore, such a dip has not been commonly found in the literature (Heller Murray *et al.*, 2020; Stepp *et al.*, 2010; Watson, 1998), perhaps because the presented data are typically averaged over and within several subjects, which might mask the transient effects.

F. Abduction initiation time and period: Sensitivity analysis

In this subsection, we study two possible sources of variability in RFF observations associated with transient effects, namely, abduction initiation time and duration of the abduction period. In this study, the choice of abduction initiation time t_i was arbitrary ($t_i = 1020$ ms). Varying t_i will initiate abduction at different phases of phonation cycle, as shown in Fig. 12, which impacts the vibration frequency. Therefore, it is important to analyze the robustness of RFF against these variations as it will contribute to gesture-to-gesture variability in RFF for a single subject, since relative abduction initiation time likely cannot be controlled with precision. Figure 13 shows that, in general, RFF profiles are sensitive to the variation in abduction initiation time with the last offset cycles tending to be less sensitive. This sensitivity is due to the fact that fundamental frequency is affected by decaying transient effects, associated with the state of the VF system at the abduction initiation time, and once these effects vanish, fundamental frequency is equal to the natural frequency of the VFs system. This implies that abduction initiation can contribute to the variability of intra-subject RFF experimental observations. Due to the robustness of the last offset cycles against varying abduction

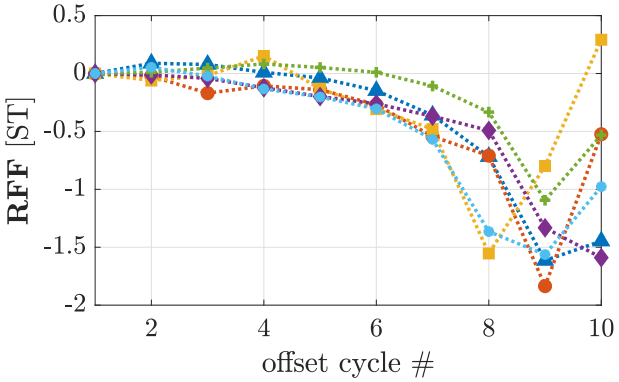

FIG. 11. (Color online) RFF profiles, based on empirical data extracted from one male subject, during the offset portions of repeated /ifi/ utterances.

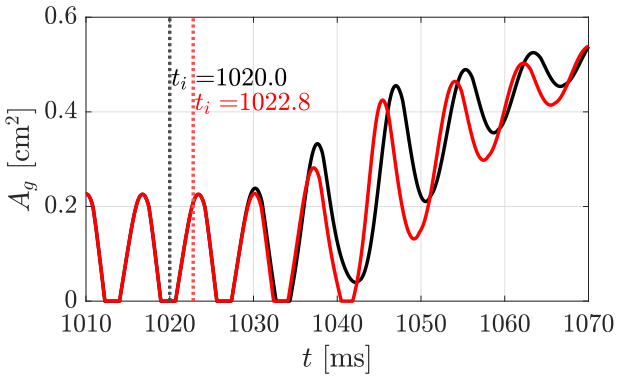

FIG. 12. (Color online) Abduction initiation at different stages of phonation cycle.

initiation time, we consider $\mathbf{RFF}(f_{\mathbf{last}})$ values in the remainder of this paper when studying different laryngeal factors.

In addition to variation in abduction initiation phase, the total duration of abduction may vary from gesture to gesture and subject to subject. In our analysis of empirical data in Sec. III D, we estimated the abduction period to be approximately $T_{\mathbf{abd}} = 80$ ms. Here, we consider different values of the duration of the abduction period $T_{\mathbf{abd}}$, with fixed abduction initiation time. Figure 14 illustrates the sensitivity of the RFF profile to the duration of the abduction period. This sensitivity is due to the changed abduction rate and that, in addition to the effect of abduction initiation time, adds to the variability of the RFF observations clinically.

G. CT muscle as a compensatory mechanism

It is understood that the CT muscle is the primary regulator of frequency during different phonation scenarios (Roubeau *et al.*, 1997). In particular, it has been found in previous studies (Titze and Story, 2002) that increasing the CT muscle activation increases fundamental frequency during sustained phonation. Therefore, the CT muscle can potentially play a role in mitigating the RFF drop during offset. To examine this potential role, we increase the CT muscle activation during offset from a minimum value, $a_{\mathbf{CT,min}}$, to a maximum value, $a_{\mathbf{CT,max}}$, rather than keeping it at a

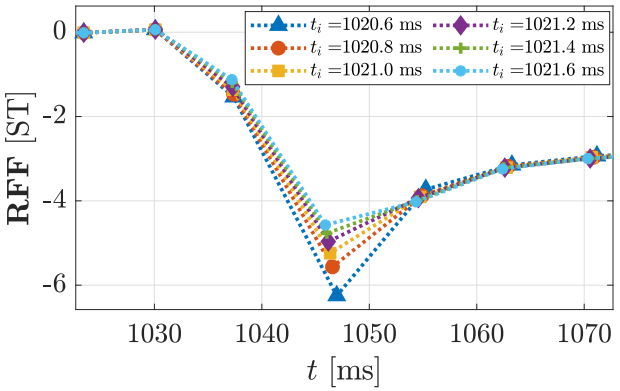

FIG. 13. (Color online) Effect of shifting abduction initiation on the RFF profile.

https://doi.org/10.1121/10.0005006

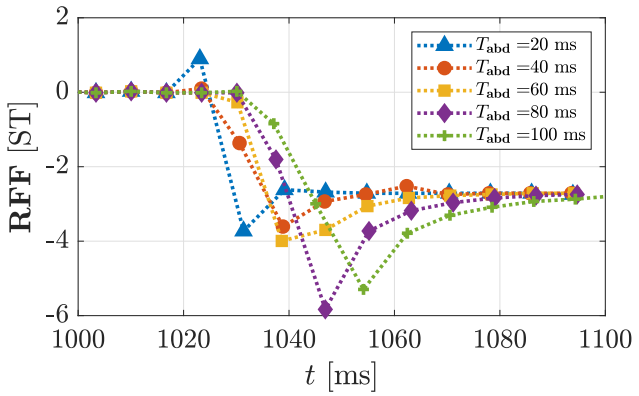

FIG. 14. (Color online) Sensitivity of the RFF profile to the duration of the abduction period.

constant value (see the inset of Fig. 15). Figure 15 shows that increasing the CT muscle activation during offset counters, in general, the drop in RFF attributed to reduced collision forces. This supports previous numerical and experimental studies that showed an increase in the CT activation, or the stiffness of the VFs, during offset in some cases (Jaiswal, 2011; Lucero and Koenig, 2005). This may explain the relatively stable fundamental frequency during phonation offset observed in healthy speakers, should CT muscle activation increase during offset in this population. Moreover, this potential role of the CT muscle may explain the sharper drop in RFF in the cases of aged and pathological speakers as CT activation in this population may be compromised (Nishida *et al.*, 2013).

H. Phonotraumatic vocal hyperfunction

Phonotraumatic vocal hyperfunction (PVH) refers to the misuse of the VFs during phonation (e.g., excessive laryngeal muscle activation, high sub-glottal pressure, etc.) resulting in benign lesions, such as polyps and nodules (Hillman *et al.*, 1989). It has been observed that speakers with PVH need to produce relatively high sub-glottal pressures during phonation to reach desired sound pressure levels, resulting in higher collision forces (Espinoza *et al.*, 2017; Kuo *et al.*, 1999).

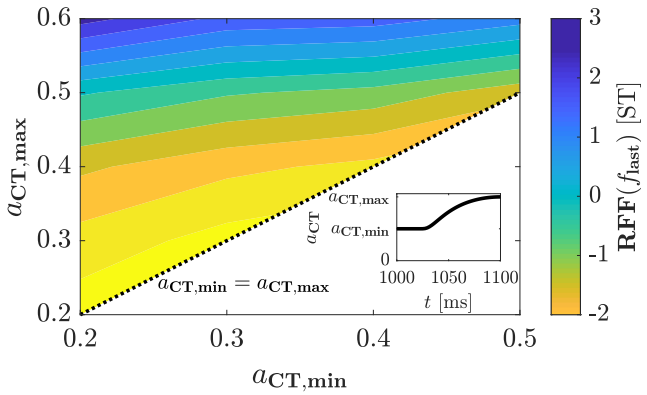

FIG. 15. (Color online) CT activation increase during abduction and its consequent effects on **RFF**(f_{last}).

In this subsection, we explore three different scenarios, associated with PVH, that produce higher collision forces and analyze the corresponding RFF behavior. The first scenario explores the impact of increasing the sub-glottal pressure. Here, we run offset simulations for various values of static sub-glottal pressure P_s and record the resulting **RFF**(f_{last}) and the maximum pre-offset collision force $F_{col,max}$. Figure 16 shows that increasing the sub-glottal pressure leads to a sharper drop in RFF, which is correlated with higher pre-offset collision forces. We note, however, that the change in **RFF**(f_{last}) and $F_{col,max}$ is relatively small over the 500 Pa range of P_s explored. We further note that the plateau in the RFF profile observed in Fig. 16 is due to the choice of the last offset cycle; for slightly longer simulation times, the RFF profile is strictly decreasing.

The second scenario explores increasing the pre-offset LCA muscle activation values. Previously, we observed how the LCA/PCA muscle activation is responsible for adducting/abducting the VFs and, subsequently, altering the collision forces. Increasing pre-offset LCA muscle activation values then represents a crude model of laryngeal tension observed in some types of vocal hyperfunction (Jiang and Titze, 1994). Specifically, we employ the same LCA muscle activation waveform, but vary the initial value, $a_{LCA,max}$, over the range of [0.45,0.53]. The final value in the LCA waveform is fixed at 0.3 for all cases, see the inset in Fig. 17. Figure 17 presents **RFF**(f_{last}) and $F_{col,max}$ as functions of $a_{LCA,max}$. The figure shows how the increased pre-offset LCA muscle activation leads to a sharper drop in RFF, which, as observed previously, is correlated with higher pre-offset maximum collision forces. We note that for the highest value of $a_{LCA,max}$ the maximum collision force actually decreases slightly, despite the continued drop in RFF, and that can be attributed, in part, to the complex dynamics of the model, which are beyond the scope of this work.

The last scenario we consider is increasing the cover mass, which corresponds to the formation of nodules or polyps (Wong *et al.*, 1991). Here, we study the effect of varying the lower cover mass, by adding a mass $\tilde{m}$ to m_1 (see Fig. 6), on **RFF**(f_{last}). Figure 18 shows that increasing the lower cover mass leads to lower RFF values, which is again

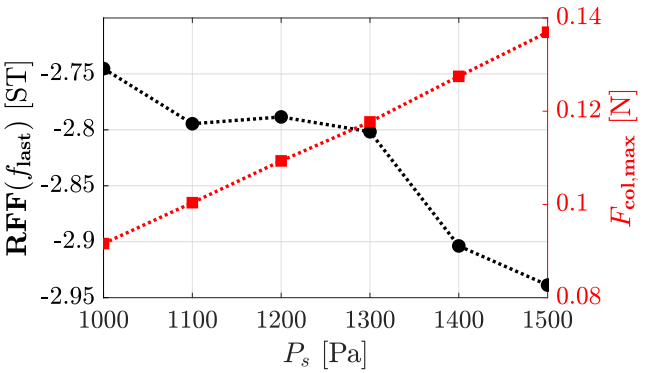

FIG. 16. (Color online) Effect of increasing sub-glottal pressure on **RFF**(f_{last}) and maximum collision force $F_{col,max}$.

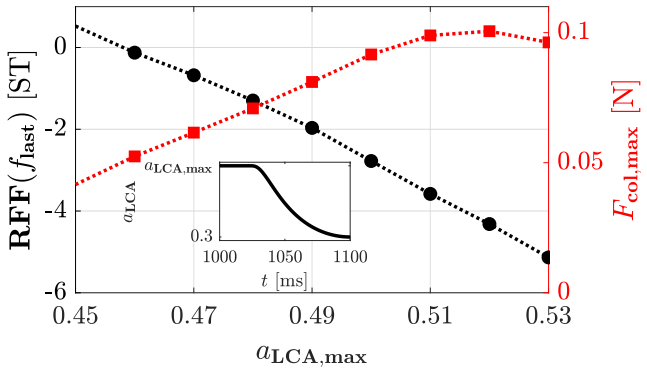

FIG. 17. (Color online) LCA muscle activation profile with varying initial values $a_{\mathbf{LCA,max}}$ and its consequent effects on $\mathbf{RFF}(f_{\mathbf{last}})$ and maximum collision force $F_{\mathbf{col,max}}$.

correlated to higher pre-offset collision forces. The increased forces can be attributed to the increased momentum of the VFs (especially prior to impact), which results in higher penetration into the collision plane and, consequently, higher collision forces. Figure 18 also indicates that the effect of increasing the cover mass on $\mathbf{RFF}(f_{\mathbf{last}})$ is insignificant, compared to, for example, the effect of pre-offset LCA muscle activation levels displayed in Fig. 17, which agrees with clinical data showing that the surgical removal of polyps and nodules does not alter RFF significantly (Stepp *et al.*, 2010).

The three scenarios considered in this subsection show how the larger drops in RFF observed clinically for subjects with PVH can be potentially attributed, at least in part, to the increased pre-offset collision forces, which can be caused by increased sub-glottal pressure, pre-offset LCA muscle activation, or additional cover mass associated with an organic pathology.

IV. CONCLUSION AND FUTURE WORK

In this work, we have introduced a theoretical and numerical framework that enabled understanding some of the laryngeal factors altering phonation frequency and RFF during phonation offset. This analysis was motivated by the promising application of RFF in assessing different voice pathologies. The main result of this work is that the clinically observed drop in RFF during offset is correlated with a decrease in collision forces as the VFs abduct. We demonstrate using a simple impact oscillator model the correlation between increased VF stiffness and sharper RFF drops observed in experimental studies. We further show that intra-subject variability in RFF may arise due to several factors, most notably the relative phase of the phonation cycle at which abduction initiates and the duration of the abduction period, which will vary from token to token and subject to subject. Moreover, we display the potential role of increasing the CT muscle activation during offset, which may be a compensatory mechanism adopted by normal speakers to stabilize frequency. Finally, we investigate possible scenarios connected to PVH showing that the clinically observed sharp RFF drops are associated with how high collision forces are prior to offset.

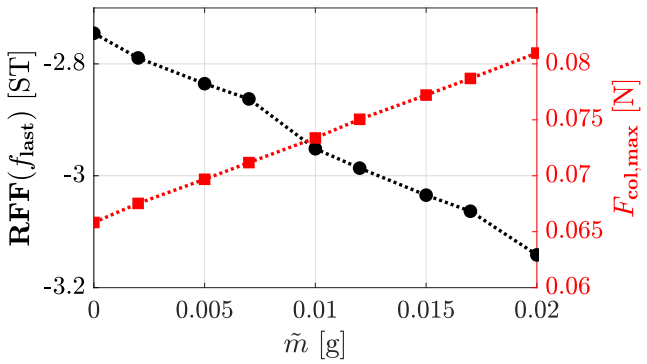

FIG. 18. (Color online) The effect of increasing the lower cover mass (by adding the mass $\tilde{m}$) on $\mathbf{RFF}(f_{\mathbf{last}})$ and $F_{\mathbf{col,max}}$.

Our study employs several assumptions to simplify our analysis of phonation offset, which include: (a) the negligible role of laryngeal muscles, other than LCA and PCA, in abducting and adducting the VFs; (b) the constant nature of sub-glottal pressure during offset, whereas it has been speculated in the literature that the profile of the sub-glottal pressure during offset is time-variant (Lucero and Koenig, 2005); and (c) the fixed supra-glottal geometry. The mentioned assumptions may limit the applicability of our findings, however, the main hypothesis of this work on how RFF and collision forces are related is not affected by these assumptions.

In future work, we aim to address the limitations introduced by the mentioned assumptions by implementing more sophisticated muscle activation rules, such as the ones proposed by Titze and Hunter (2007), and considering the time varying nature of sub-glottal pressure and supra-glottal vocal tract. Moreover, we aim at developing more advanced theoretical models of abduction that are capable of capturing the transient nature of the neutral gap, which can enable better understanding of the offset dynamics. Finally, we aim to develop models that capture the physiological aspects of different voice pathologies, and in particular nonphonotraumatic vocal hyperfunction, and to explore the underlying mechanisms associated with such pathologies.

ACKNOWLEDGMENTS

Research reported in this work was supported by the NIDCD of the NIH under Award Nos. P50DC015446 and R01DC015570. The content is solely the responsibility of the authors and does not necessarily represent the official views of the National Institutes of Health.

APPENDIX A: DERIVATION OF THE FREQUENCY FORMULA

Let ϕ denote the solution to Eq. (2), with $\phi(t_0) = 0$, $\dot{\phi}(t_0) = v_0 = \sqrt{2E_0/M}$, in the collision-free interval $[t_0, t_2]$, see Fig. 2. Then, ϕ is given explicitly by $\phi(t) = v_0\sqrt{M/K}\sin\left(\sqrt{K/M}(t - t_0)\right)$, $t \in [t_0, t_2]$. The term

https://doi.org/10.1121/10.0005006

$t_f = t_1 - t_0$ is obtained by solving the algebraic equation $\phi(t_f + t_0) = 0$, which results in $t_f = \pi\sqrt{M/K}$. Moreover, the term $t_\delta = t_2 - t_1$ can be obtained by solving the algebraic equation $\phi(t_\delta + t_0) = \delta$, which has the explicit solution $t_\delta = \sqrt{M/K}\arcsin(\delta)$. To obtain an analytic expression of the contact time t_c, let $\eta(t) = -(\xi(t) + \delta)$ be the displacement beyond the collision plane; then Eq. (3) can be rewritten as

$$M\ddot{\eta} + (K + k_{\mathbf{col}})\eta = -K\delta,\ \eta(t) > 0. \tag{A1}$$

Deriving an analytical expression of t_c requires solving Eq. (A1) over the interval $[t_2, t_3]$ in the collision regime. The velocity prior to the collision, $v_{\mathbf{col}}$, can be obtained from the energy equation $2E_0 = K\delta^2 + Mv_{\mathbf{col}}^2$ resulting in $v_{\mathbf{col}} = \sqrt{(2E_0 - K\delta^2)/M}$. Now, let ψ be the solution to Eq. (A1), over the interval $[t_2, t_3]$ with $\psi(t_2) = 0$ and $\dot{\psi}(t_2) = v_{\mathbf{col}}$, which is given explicitly as $\psi(t) = \tilde{k}\delta(C\sin(\omega(t - t_2)) + \cos(\omega(t - t_2)) - 1)$, $t \in [t_2, t_3]$, where $\omega = \sqrt{(K + k_{\mathbf{col}})/M}$ and $C = \sqrt{(1/\tilde{\delta}^2 - 1)/\tilde{k}}$. Direct substitution of ψ into Eq. (A1) demonstrates that it is indeed a solution to the ODE. Then, t_c is obtained by solving the algebraic equation $\psi(t_c + t_2) = 0$, which has the analytic solution $t_c = 2\arctan(C)/\omega$.

APPENDIX B: FUNDAMENTAL FREQUENCY BOUNDS

The upper bound follows easily from the fact that $\arctan(x), \arcsin(x) \geq 0$ for all $x \geq 0$. The lower bound is obtained as follows: note that for all $y \in (0, 1]$ and all $x \in [0, \infty)$, $y\arctan(x/y) \leq \arctan(x)$. This inequality can be obtained by comparing the integrands of $\arctan(x) = \int_0^x 1/(1 + t^2)\,\mathrm{d}t$ and $y\arctan(x/y) = \int_0^x 1/(1 + (t/y)^2)\,\mathrm{d}t$. Using this inequality in the expression of f results in the inequality $f \geq 2f_0/([2/\pi]\arctan\sqrt{1/\tilde{\delta}^2 - 1} + [2/\pi]\arcsin(\tilde{\delta}) + 1) = g$. Moreover, using the identity $\arctan\left(\sqrt{1 - x^2}/x\right) = \pi/2 - \arcsin(x)$, $x > 0$, in the expression of g simplifies it to be $g = f_0$.

APPENDIX C: MAXIMUM COLLISION FORCE

As the collision forces in the collision regime are linearly elastic, we need to find the maximum displacement $\eta_{\mathbf{max}}$ beyond the collision plane. To do so, we resort to the energy equation [deduced from Eq. (A1) by integrating both sides with respect to η] $M\dot{\eta}(\tau_1)^2/2 + (K + k_{\mathbf{col}})\eta(\tau_1)^2/2 + K\delta\eta(\tau_1) = M\dot{\eta}(\tau_2)^2/2 + (K + k_{\mathbf{col}})\eta(\tau_2)^2/2 + K\delta\eta(\tau_2), \tau_1, \tau_2 \in [t_2, t_3]$. Let $\tau_1 = t_2$ (beginning of collision) and τ_2 be the time instance corresponding to the maximum displacement $\eta_{\mathbf{max}}$. Note that at τ_1, $\eta(\tau_1) = 0$ and $\dot{\eta}(\tau_1) = v_{\mathbf{col}} = \sqrt{(2E_0 - K\delta^2)/M}$, and at τ_2, $\eta(\tau_2) = \eta_{\mathbf{max}}$ and $\dot{\eta}(\tau_2) = 0$. Consequently, we have $(K + k_{\mathbf{col}})\eta_{\mathbf{max}}^2 + 2K\delta\eta_{\mathbf{max}} - Mv_{\mathbf{col}}^2 = 0$, which results in $\eta_{\mathbf{max}} = \tilde{k}\delta(-1 + \sqrt{1 + (1/\tilde{\delta}^2 - 1)/\tilde{k}})$. Substituting the formula of $\eta_{\mathbf{max}}$ into the formula $F_{\mathbf{col,max}} = k_{\mathbf{col}}\eta_{\mathbf{max}}$ and rearranging results in Eq. (5).

[1]Empirical data, obtained under NIH award R01DC015570, were provided by the STEPP lab at Boston University. For details on the data collection methodology, including IRB approval information, see Diaz-Cadiz *et al.* (2019).

Berry, D. A., and Titze, I. R. (**1996**). "Normal modes in a continuum model of vocal fold tissues," J. Acoust. Soc. Am. **100**(5), 3345–3354.

Diaz-Cadiz, M., McKenna, V. S., Vojtech, J. M., and Stepp, C. E. (**2019**). "Adductory vocal fold kinematic trajectories during conventional versus high-speed videoendoscopy," J. Speech Lang. Hear. Res. **62**, 1685–1706.

Erath, B. D., Zanartu, M., Stewart, K. C., Plesniak, M. W., Sommer, D. E., and Peterson, S. D. (**2013**). "A review of lumped-element models of voiced speech," Speech Commun. **55**(5), 667–690.

Espinoza, V. M., Zañartu, M., Van Stan, J. H., Mehta, D. D., and Hillman, R. E. (**2017**). "Glottal aerodynamic measures in women with phonotraumatic and nonphonotraumatic vocal hyperfunction," J. Speech Lang. Hear. Res. **60**(8), 2159–2169.

Galindo, G. E., Peterson, S. D., Erath, B. D., Castro, C., Hillman, R. E., and Zañartu, M. (**2017**). "Modeling the pathophysiology of phonotraumatic vocal hyperfunction with a triangular glottal model of the vocal folds," J. Speech Lang. Hear. Res. **60**(9), 2452–2471.

Galindo, G. E., Zanartu, M., and Yuz, J. I. (**2014**). "A discrete-time model for the vocal folds," in *Proceedings of IEEE Engineering in Medicine and Biology Society International Student Conference*, pp. 74–77.

Goberman, A. M., and Blomgren, M. (**2008**). "Fundamental frequency change during offset and onset of voicing in individuals with Parkinson disease," J. Voice **22**(2), 178–191.

Grace, I., and Ibrahim, R. (**2008**). "Modelling and analysis of ship roll oscillations interacting with stationary icebergs," Proc. Inst. Mech. Eng. Part C: J. Mech. Eng. Sci. **222**(10), 1873–1884.

Hadwin, P. J., Galindo, G. E., Daun, K. J., Zañartu, M., Erath, B. D., Cataldo, E., and Peterson, S. D. (**2016**). "Non-stationary Bayesian estimation of parameters from a body cover model of the vocal folds," J. Acoust. Soc. Am. **139**(5), 2683–2696.

Hanson, H. M. (**2009**). "Effects of obstruent consonants on fundamental frequency at vowel onset in English," J. Acoust. Soc. Am. **125**(1), 425–441.

Heller Murray, E. S., Lien, Y.-A. S., Van Stan, J. H., Mehta, D. D., Hillman, R. E., Pieter Noordzij, J., and Stepp, C. E. (**2017**). "Relative fundamental frequency distinguishes between phonotraumatic and nonphonotraumatic vocal hyperfunction," J. Speech Lang. Hear. Res. **60**(6), 1507–1515.

Heller Murray, E. S., Segina, R. K., Woodnorth, G. H., and Stepp, C. E. (**2020**). "Relative fundamental frequency in children with and without vocal fold nodules," J. Speech Lang. Hear. Res. **63**, 361–371.

Henríquez, P., Alonso, J. B., Ferrer, M. A., Travieso, C. M., Godino-Llorente, J. I., and Díaz-de María, F. (**2009**). "Characterization of healthy and pathological voice through measures based on nonlinear dynamics," IEEE Trans. Audio Speech Lang. Process. **17**(6), 1186–1195.

Hillman, R. E., Holmberg, E. B., Perkell, J. S., Walsh, M., and Vaughan, C. (**1989**). "Objective assessment of vocal hyperfunction: An experimental framework and initial results," J. Speech Lang. Hear. Res. **32**(2), 373–392.

Ing, J., Pavlovskaia, E., Wiercigroch, M., and Banerjee, S. (**2008**). "Experimental study of impact oscillator with one-sided elastic constraint," Philos. Trans. R. Soc. A: Math. Phys. Eng. Sci. **366**(1866), 679–705.

Jaiswal, S. (**2011**). "Cricothyroid muscle activity at voicing transitions," Ph.D. thesis, University of Iowa, Iowa City, IA.

Jiang, J. J., and Titze, I. R. (**1994**). "Measurement of vocal fold intraglottal pressure and impact stress," J. Voice **8**(2), 132–144.

Jiang, J. J., Zhang, Y., MacCallum, J., Sprecher, A., and Zhou, L. (**2009**). "Objective acoustic analysis of pathological voices from patients with vocal nodules and polyps," Folia Phon. Logop. **61**(6), 342–349.

Jiang, J. J., Zhang, Y., and McGilligan, C. (**2006**). "Chaos in voice, from modeling to measurement," J. Voice **20**(1), 2–17.

Kelly, J. L., and Lochbaum, C. C. (**1962**). "Speech synthesis," in *Proceedings of the Fourth International Congress on Acoustics*.

Kuo, J., Holmberg, E. B., and Hillman, R. E. (**1999**). "Discriminating speakers with vocal nodules using aerodynamic and acoustic features," in *Proceedings of the 1999 IEEE International Conference on Acoustics, Speech, and Signal Processing (ICASSP99)* (IEEE, New York), Vol. 1, pp. 77–80.
Lien, Y. S., Calabrese, C. R., Michener, C. M., Heller Murray, E., Van Stan, J. H., Mehta, D. D., Hillman, R. E., Noordzij, J. P., and Stepp, C. E. (**2015**). "Voice relative fundamental frequency via neck-skin acceleration in individuals with voice disorders," J. Speech Lang. Hear. Res. **58**(5), 1482–1487.
Lien, Y. A. S., Heller Murray, E. S., Calabrese, C. R., Michener, C. M., Van Stan, J. H., Mehta, D. D., Hillman, R. E., Noordzij, J. P., and Stepp, C. E. (**2017**). "Validation of an algorithm for semi-automated estimation of voice relative fundamental frequency," Ann. Otol. Rhinol. Laryngol. **126**(10), 712–716.
Liljencrants, J. (**1985**). "Speech synthesis with a reflection-type line analog," Ph.D. thesis, Royal Institute of Technology, Stockholm, Sweden.
Lucero, J. C., and Koenig, L. L. (**2005**). "Phonation thresholds as a function of laryngeal size in a two-mass model of the vocal folds," J. Acoust. Soc. Am. **118**(5), 2798–2801.
McKenna, V. S., Heller Murray, E. S., Lien, Y.-A. S., and Stepp, C. E. (**2016**). "The relationship between relative fundamental frequency and a kinematic estimate of laryngeal stiffness in healthy adults," J. Speech Lang. Hear. Res. **59**(6), 1283–1294.
Nagurka, M., and Huang, S. (**2004**). "A mass-spring-damper model of a bouncing ball," in *Proceedings of the 2004 American Control Conference* (IEEE, New York), Vol. 1, pp. 499–504.
Newmark, N. M. (**1959**). "A method of computation for structural dynamics," J. Eng. Mech. Div. **85**(3), 67–94.
Nishida, N., Taguchi, A., Motoyoshi, K., Hyodo, M., Gyo, K., and Desaki, J. (**2013**). "Age-related changes in rat intrinsic laryngeal muscles: Analysis of muscle fibers, muscle fiber proteins, and subneural apparatuses," Eur. Arch. Oto-Rhino-Laryngol. **270**(3), 975–984.
Nordmark, A. B. (**1991**). "Non-periodic motion caused by grazing incidence in an impact oscillator," J. Sound Vib. **145**(2), 279–297.
Ohde, R. N. (**1984**). "Fundamental frequency as an acoustic correlate of stop consonant voicing," J. Acoust. Soc. Am. **75**(1), 224–230.
Roubeau, B., Chevrie-Muller, C., and Saint Guily, J. L. (**1997**). "Electromyographic activity of strap and cricothyroid muscles in pitch change," Acta Oto-laryngol. **117**(3), 459–464.
Senator, M. (**1970**). "Existence and stability of periodic motions of a harmonically forced impacting system," J. Acoust. Soc. Am. **47**(5B), 1390–1397.
Shaw, S. W., and Holmes, P. (**1983**). "A periodically forced piecewise linear oscillator," J. Sound Vib. **90**(1), 129–155.
Smith, A. B., and Robb, M. P. (**2013**). "Factors underlying short-term fundamental frequency variation during vocal onset and offset," Speech Lang. Hear. **16**(4), 208–214.
Steinecke, I., and Herzel, H. (**1995**). "Bifurcations in an asymmetric vocal-fold model," J. Acoust. Soc. Am. **97**(3), 1874–1884.
Stepp, C. E., Hillman, R. E., and Heaton, J. T. (**2010**). "The impact of vocal hyperfunction on relative fundamental frequency during voicing offset and onset," J. Speech Lang. Hear. Res. **53**, 1220–1226.
Story, B. H. (**2002**). "An overview of the physiology, physics and modeling of the sound source for vowels," Acoust. Sci. Technol. **23**(4), 195–206.
Story, B. H. (**2005**). "A parametric model of the vocal tract area function for vowel and consonant simulation," J. Acoust. Soc. Am. **117**(5), 3231–3254.
Story, B. H., and Titze, I. R. (**1995**). "Voice simulation with a body-cover model of the vocal folds," J. Acoust. Soc. Am. **97**(2), 1249–1260.
Takemoto, H., Honda, K., Masaki, S., Shimada, Y., and Fujimoto, I. (**2006**). "Measurement of temporal changes in vocal tract area function from 3D CINE-MRI data," J. Acoust. Soc. Am. **119**(2), 1037–1049.
Titze, I. R. (**1989**). "On the relation between subglottal pressure and fundamental frequency in phonation," J. Acoustical Soc. America **85**(2), 901–906.
Titze, I., and Alipour, F. (**2006**). *The Myoelastic-Aerodynamic Theory of Phonation* (National Center for Voice and Speech, Iowa City, IA).
Titze, I. R., and Hunter, E. J. (**2004**). "Normal vibration frequencies of the vocal ligament," J. Acoust. Soc. Am. **115**(5), 2264–2269.
Titze, I. R., and Hunter, E. J. (**2007**). "A two-dimensional biomechanical model of vocal fold posturing," J. Acoust. Soc. Am. **121**(4), 2254–2260.
Titze, I. R., and Story, B. H. (**2002**). "Rules for controlling low-dimensional vocal fold models with muscle activation," J. Acoust. Soc. Am. **112**(3), 1064–1076.
Vojtech, J. M., Segina, R. K., Buckley, D. P., Kolin, K. R., Tardif, M. C., Noordzij, J. P., and Stepp, C. E. (**2019**). "Refining algorithmic estimation of relative fundamental frequency: Accounting for sample characteristics and fundamental frequency estimation method," J. Acoust. Soc. Am. **146**(5), 3184–3202.
Watson, B. C. (**1998**). "Fundamental frequency during phonetically governed devoicing in normal young and aged speakers," J. Acoust. Soc. Am. **103**(6), 3642–3647.
Weibel, E. R., Cournand, A. F., and Richards, D. W. (**1963**). *Morphometry of the Human Lung* (Springer, Berlin).
Wong, D., Ito, M. R., Cox, N. B., and Titze, I. R. (**1991**). "Observation of perturbations in a lumped-element model of the vocal folds with application to some pathological cases," J. Acoust. Soc. Am. **89**(1), 383–394.
Zanartu, M. (**2006**). "Influence of acoustic loading on the flowinduced oscillations of single mass models of the human larynx," Master's thesis, Purdue University, West Lafayette, IN.
Zañartu, M., Galindo, G. E., Erath, B. D., Peterson, S. D., Wodicka, G. R., and Hillman, R. E. (**2014**). "Modeling the effects of a posterior glottal opening on vocal fold dynamics with implications for vocal hyperfunction," J. Acoust. Soc. Am. **136**(6), 3262–3271.
Zhang, K., Siegmund, T., and Chan, R. W. (**2006**). "A constitutive model of the human vocal fold cover for fundamental frequency regulation," J. Acoust. Soc. Am. **119**(2), 1050–1062.